Continuous measurement of diffusive and ebullitive fluxes of methane in aquatic ecosystems by an open dynamic chamber method

Oscar Gerardo-Nieto,[†] Abner Vega-Peñaranda,[‡] Rodrigo Gonzalez-Valencia,[†] Yameli Alfano-Ojeda,[†] Frederic Thalasso[,†]*

†Biotechnology and Bioengineering Department, Cinvestav, Mexico City, Av. IPN 2508, San Pedro Zacatenco, MX 07360, Mexico

‡ University of Francisco de Paula Santander, Av. Gran Colombia 12E-96, San José de Cúcuta, Colombia

Supporting information

Number of SI pages: 14
Number of SI figures: 7
Number of SI Tables: 4

S1. Literature review

Table S1. List of previous reports on the use of ODC (ordered chronologically).

Ecosystem	Gas analyzed	Author	Year
Soil	CO_2	Edward & Sollins[1]	1973
Soil	N_2O	Denmead[2]	1979
Soil	NH_3	Svensson [3]	1994
Soil	CO_2	Fang & Moncrieff[4]	1996
Soil	CH_3Br	Gao *et al.*[5]	1997
Soil	CH_2Cl_2	Gao & Yates[6]	1998
Soil	VOC	Gao & Yates[7]	1998
Soil	Hg	Carpi & Lindberg[8]	1998
Soil	Hg	Zhang *et al.*[9]	2002
Soil	Hg	Lindberg *et al.*[10]	2002
Soil	NO	Tabachow *et al.*[11]	2002
Soil	VOC	Reichman & Rolston[12]	2002
Soil	CO_2	Pumpanen *et al.*[13]	2004
Soil	CH_4, N_2O	Denmead[14]	2008
Soil	CO_2, H_2O, NO, NO_2, O_3	Pape *et al.*[15]	2009
Plants	NO, NO_2, O_3	Breuninger *et al.*[16]	2012
Peatland	CH_4	Yu *et al.*[17]	2014
Soil	H_2O	Marasco *et al.*[18]	2014
Soil	BTEX	Verginelli *et al.*[19]	2018

S2. ODC characteristics

Table S2. Main power and gas requirements, autonomy and approximate cost of the ODC method, as used in the present work.

Power requirement (12 V)	60	W
Energy autonomy (50 Ah car battery)	8-10	h
CH_4-free nitrogen flow rate	7.7	L min^{-1}
Autonomy "BT-80" cylinder (2300 L capacity)	5.0	h
UGGA datalogger autonomy	>100	d
UGGA (approximate cost)	40000	US$
Mass flow controller (approximate cost)	1000	US$
Battery, chamber, tubing and accessories (approximate cost)	300	US$

S3. Flowchart and mass balance equations

The flowchart of the ODC method is shown in Figure S1. Our model considers that the gas phase is fully mixed, both in the chamber and in the spectrometer cavity. Although in the present work we used CH_4– and CO_2–free nitrogen as carrier gas, the model considers an input concentration for increased versatility.

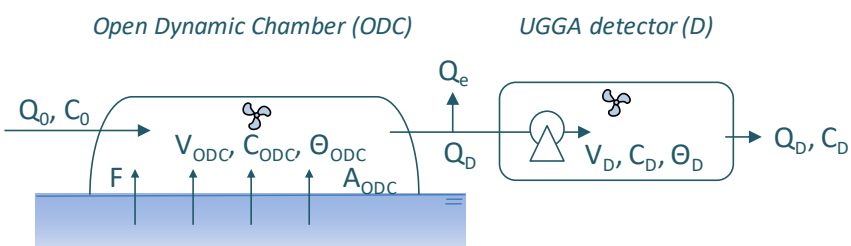

Figure S1: Flowchart of the ODC method.

Where:

F: CH_4 flux (g m^{-2} s^{-1}),
C_0: Influent carrier gas concentration (g m^{-3})
C_{ODC}: Gas concentration in the ODC (g m^{-3})
C_D: Measured concentration in the UGGA spectrometer (g m^{-3})
Q_0: Carrier gas influent flow rate (m^3 h^{-1})
Q_e: Purge, excess flow rate (m^3 h^{-1})
Q_D: Flow rate extracted by the spectrometer (m^3 h^{-1})
A_{ODC}: Area of the dynamic chamber in contact with the ecosystem (m^2)
V_{ODC}: Volume of the dynamic chamber (m^3)
V_D: Volume of the spectrometer cavity (m^3)
Θ_{ODC}: Gas residence time in the dynamic chamber (s)
Θ_D: Gas residence time in the spectrometer cavity (s)

Assuming that the concentration in the spectrometer cavity (C_D) is homogeneous, the mass balance in that cavity can be described by:

$$\frac{dC_D}{dt} = \frac{Q_D}{V_D} \cdot C_{ODC} - \frac{Q_D}{V_D} \cdot C_D \qquad \text{(S1)}$$

In turn, assuming that the cavity of the spectrometer is fully mixed, the residence time (Θ_D) can be described by:

$$\frac{1}{\Theta_D} = \frac{Q_D}{V_D} \qquad \text{(S2)}$$

Such that we can write:

$$\frac{dC_D}{dt} = \frac{1}{\Theta_D} \cdot (C_{ODC} - C_D) \qquad \text{(S3)}$$

$$C_{ODC} = \Theta_D \frac{dC_D}{dt} + C_D \qquad \text{(S4)}$$

Equation S4 allows the determination of C_{ODC}, at any time, from spectrometer measurements. Similarly, assuming that the headspace of the Open Dynamic Chamber is fully mixed, the mass balance can be described by:

$$\frac{dC_{ODC}}{dt} = \frac{Q_0}{V_{ODC}} \cdot C_0 - \frac{Q_e}{V_{ODC}} \cdot C_{ODC} - \frac{Q_D}{V_{ODC}} \cdot C_{ODC} + F \cdot \frac{A_{ODC}}{V_{ODC}} \qquad \text{(S5)}$$

Assuming mass conservation, the influent flow (Q_0) equals the sum of the effluent flows (Q_e + Q_D), and Eq. S5 can be rewritten as follows:

$$\frac{dC_{ODC}}{dt} = \frac{Q_0}{V_{ODC}} \cdot (C_0 - C_{ODC}) + F \cdot \frac{A_{ODC}}{V_{ODC}} \qquad \text{(S6)}$$

The residence time in dynamic chamber (Θ_{ODC}) can be described by:

$$\frac{1}{\Theta_{ODC}} = \frac{Q_0}{V_{ODC}} \qquad \text{(S7)}$$

By rearranging Eq. S6, we obtain:

$$F = \left(\frac{dC_{ODC}}{dt} + \frac{C_{ODC} - C_0}{\Theta_{ODC}}\right) \cdot \frac{V_{ODC}}{A_{ODC}} \qquad \text{(S8)}$$

Which, in combination with Eq. S4, results in:

$$F = \left(\frac{d\left(\Theta_D \frac{dC_D}{dt} + C_D\right)}{dt} + \frac{\Theta_D \frac{dC_D}{dt} + C_D - C_0}{\Theta_{ODC}}\right) \cdot \frac{V_{ODC}}{A_{ODC}} \qquad \text{(S9)}$$

Thus, Equation S9 allows the measurement of instantaneous flux from spectrometer measurements. It is important to note that the UGGA detector measures gas concentrations in ppm ($C_{D,ppm}$), whereas in Equation S9 the concentrations are expressed in g m^{-3}. To convert $C_{D,ppm}$ we used Equations S10 and S11; where M_{CH4} is the molar weight of CH_4 (16 g mol^{-1}), V_M is the molar volume of the gas of interest (m^3 mol^{-1}; Eq. S11), 1,000,000 is the conversion factor from ppm to vol./vol., P is the atmospheric pressure during measurements (Atm), R is the universal gas constant (8.2058 10^{-5} m^3 Atm K^{-1} Mol^{-1}), and T is the absolute temperature during measurements (K):

$$C_D = \frac{C_{D,ppm}}{1{,}000{,}000} \cdot \frac{M_{CH4}}{V_M} \quad \text{(S10)}$$

$$V_M = \frac{R.T}{P} \quad \text{(S11)}$$

S4. Data processing.

S4.1. Flux measurement

During field application of the ODC method, as described above, we established the best method for data processing as a combination of flux determination and bubble characterization. The strategy is described in Figure S4, on the basis of an actual measurement made at a highly ebullitive region of LG. After calibration, the ODC was positioned on the surface of the ecosystem. About 30 s were required for the system to stabilize. Then, C_D was continuously acquired at a frequency of 1 Hz. Data treatment consisted, first, in the detection of ebullitive event and the characterization of bubbles, according to Equations 4−7. Then, C_D measurements were converted to flux (Eq. 1), which were smoothened (Eqs. 1–3).

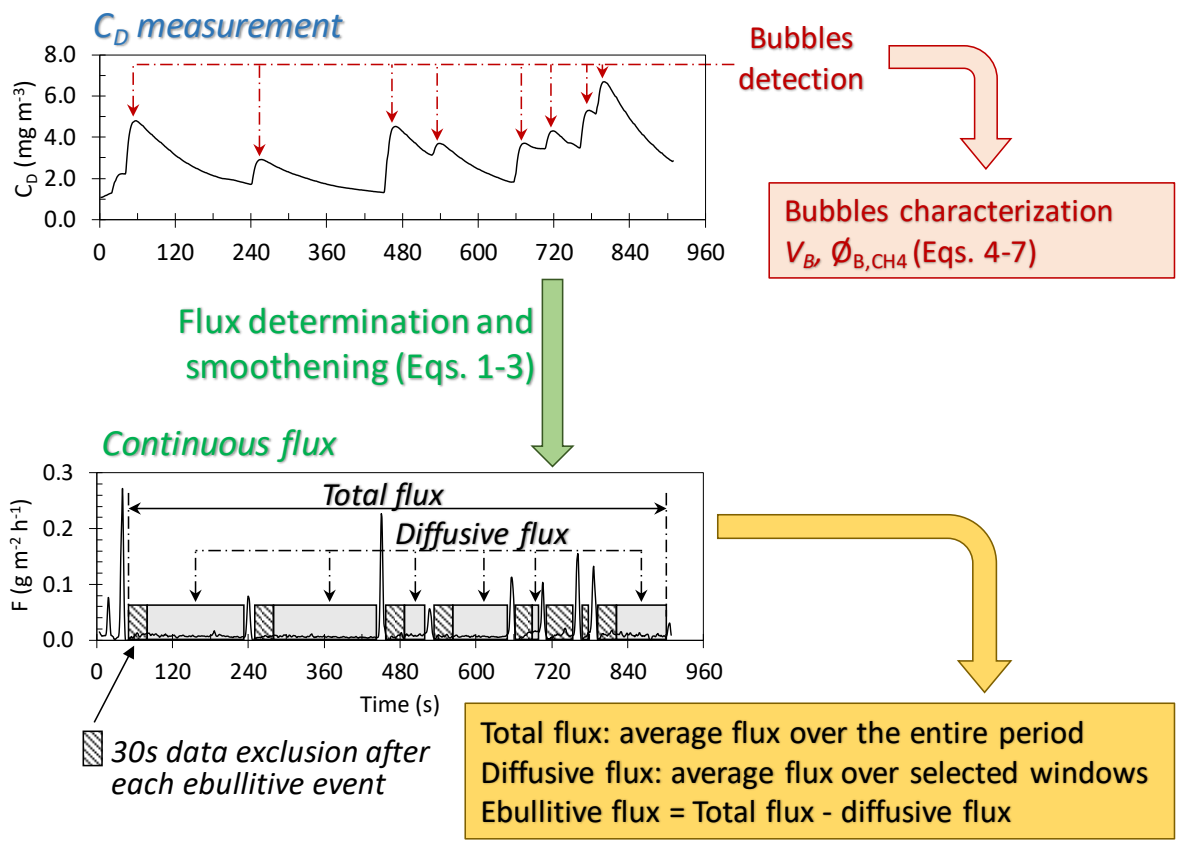

Figure S2: Sequence of data processing.

As shown in the Results and Discussion section, just after an ebullition event, a significant instability was observed in flux data for 10−15 s, which corresponded to the period during which the C_D concentration was reaching the peak concentration and returning to a decreasing trend. Consequently, to reduce errors in diffusive flux calculations, we decided to discard 30 s of data after each ebullitive event. As shown in Figure S2, total flux was then determined as the average of the complete set of flux data (without exclusion periods), while diffusive flux was determined as the average of diffusive flux over the selected periods, and ebullitive flux was determined from the difference between total and diffusive flux.

S4.2. SNR measurement

SNR of C_D was calculated as follows; first, we selected 10 min regions of the data sets obtained from the laboratory and field deployment where steady state was observed; i.e., absence of ebullition and visible trend, and final C_D values not significantly different than initial values. Second, the SNR was calculated from the standard deviations and means of 15 C_D data.

S5. Bubbles characterization

As shown in the results sections, instantaneous total flux was successfully determined with Equation S9. Ebullitive events were clearly detectable by an abrupt and short increase in flux. However, a significant noise in the instantaneous flux determination was observed, particularly when two ebullitive events were occurring in a short period of time, resulting in a significant error and impeding the precise determination of the bubbles characteristics. Therefore, a different strategy was implemented, which was based on the determination of the maximum concentration observed after an ebullitive event, instead of the instantaneous flux determination. Figure S2 illustrates the concentration observed in the ODC and in the cavity of the UGGA detector during a double ebullitive event. This simulation was done, using the mass balance equations (Eq. S1 and S6; Figure S3), to illustrate the strategy used for the characterization of bubbles, presented in the main document.

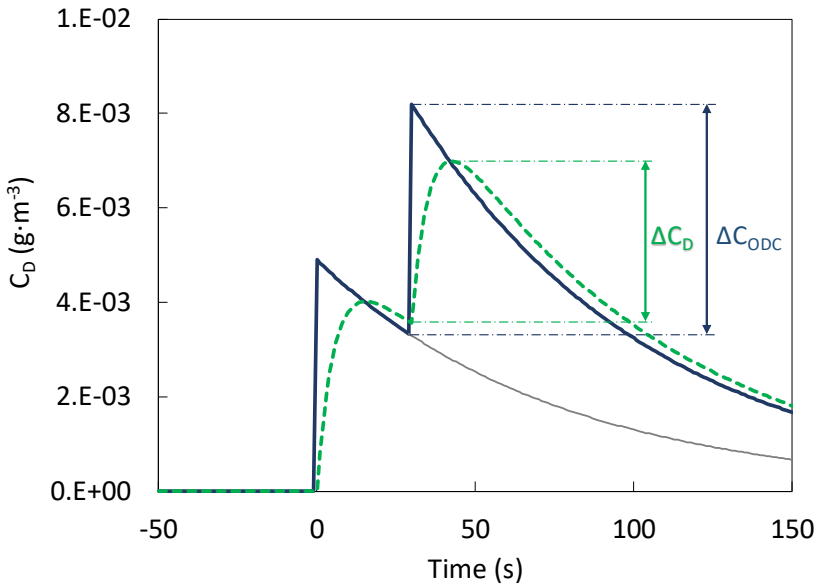

Figure S3: Theoretical simulation of the concentration observed in the Chamber (C_{ODC}; —) and in the UGGA detector (C_D; ---), that would be observed during a double ebullitive event with a 30 s interval. This simulation was obtained from mass balance equations, under the following conditions; bubbles diameter, 5 mm; bubble composition, 100% CH_4; Θ_{ODC}, 76 s; Θ_D, 6 s; T, 293.15 K, P, 1 atm.

S6 Laboratory testing.

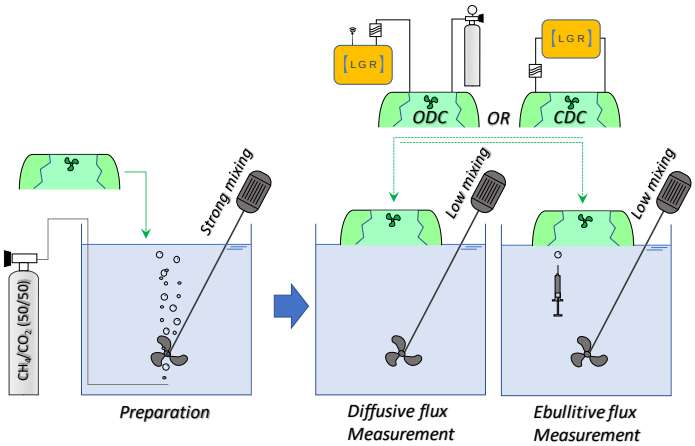

Figure S4: Experimental set-up for laboratory testing.

S7 Results and discussion

S7.1 CH_4 flux measurements

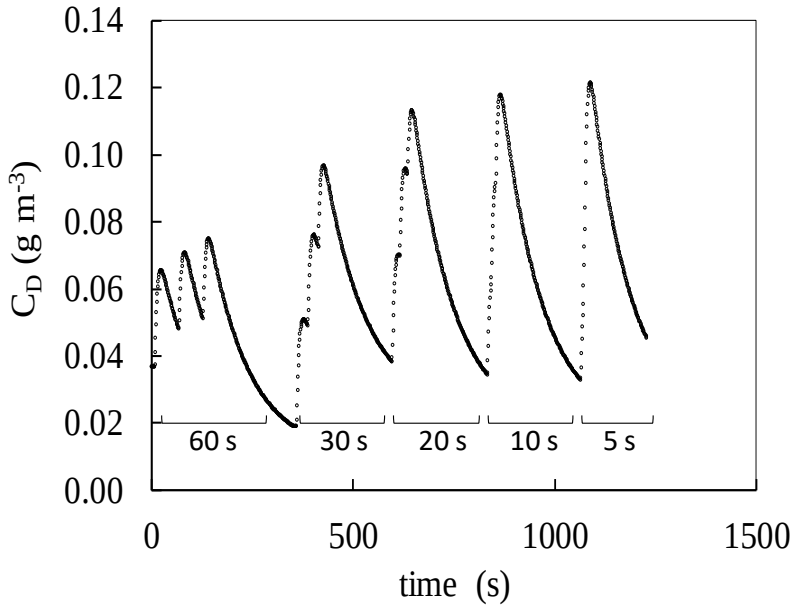

Figure S5: CH_4 concentration (C_D) observed during the injection of three 2 mL bubbles (CH_4/CO_2; 60/40%vol.) with an interval of 60, 30, 20, 10 and 5 s.

S7.2 CO_2 flux measurements

First, we tested the ODC method in the laboratory, for CO_2 diffusive fluxes and for the characterization of bubbles, as previously done for CH_4 (Figs. 2 and 3). The results (not shown) were similar to those observed with CH_4 (in both cases $R^2 > 0.96$). However, during the field deployment, we observed noisier signals from the UGGA, which were quantified through an SNR of 343 ± 82, which was significantly lower than that observed with CH_4. In LG, the correlation between diffusive fluxes measured with the standard CDC and the ODC was significant (R^2 of 0.92, $p < .01$); in LL, however, erratic results were observed. Undoubtedly, the failure of the method in LL was caused by the relatively low UGGA sensitivity to CO_2 (reported by the manufacturer to be 1 ppm). The mean CO_2 diffusive flux in LG and LL, measured with the standard CDC, was 70.9 ± 26 and 3.0 ± 2.5 mg m^{-2} h^{-1}, respectively. These CO_2 fluxes corresponded to a C_D of 28.3 ± 10.4 and 1.21 ± 1.00 ppm, respectively. Thus, in LG, the CO_2 flux was in the region of the UGGA detection limit (1 ppm). From these results, we arbitrarily estimated that the limit of detection of the ODC method was about 10 mg CO_2 m^{-2} h^{-1}, which corresponded to a C_D of 4 ppm. This minimum flux that can be measured is higher than the lower range of CO_2 fluxes reported by Rasilo et al.[20] in 224 lakes.

During the combined diffusive and ebullitive flux measurements in LG, we observed abrupt increases in C_D and their corresponding CO_2 peaks in the flux data (Fig. S7). However, in this case, to distinguish peak fluxes from the background noise, we needed a cut-off index for an instantaneous flux of 2.15 g CO_2 m^{-2} h^{-1}, which corresponds to a bubble content of 31.2×10^{-3} mL of CO_2 or to bubbles of 12.6– 18.1 mm in diameter if they contain 3–1% CO_2. This range is above the higher range of bubble diameters previously reported in lakes, 2.6–11.4 mm,[21–24] which indicates that the ODC method, under the experimental conditions tested, presents serious limitations. The latter was confirmed by our field experiments, as CO_2 was detected only in the largest bubbles. Supposing that the bubbles were only composed of CH_4 and CO_2; i.e. the two gases detected by the UGGA, the smallest bubble with CO_2 detected (0.29 mL total volume or 8.2 mm diameter) contained 17% CO_2. Only 23 bubbles (27%) containing CO_2 were detected out of the 84 with a volume >0.29 mL. These bubbles contained, on average, 8.5% CO_2. Clearly, these percentages are not representative of the entire bubble population, but only of the largest bubbles containing a mass of CO_2 above the detection limit of the method. Thus, the CO_2 percentages reported here are significantly higher than most previous reports in the literature; i.e., 0.1–3%,[25–27] although Poissant et al.[28] reported a range of 5–15% CO_2 in a river.

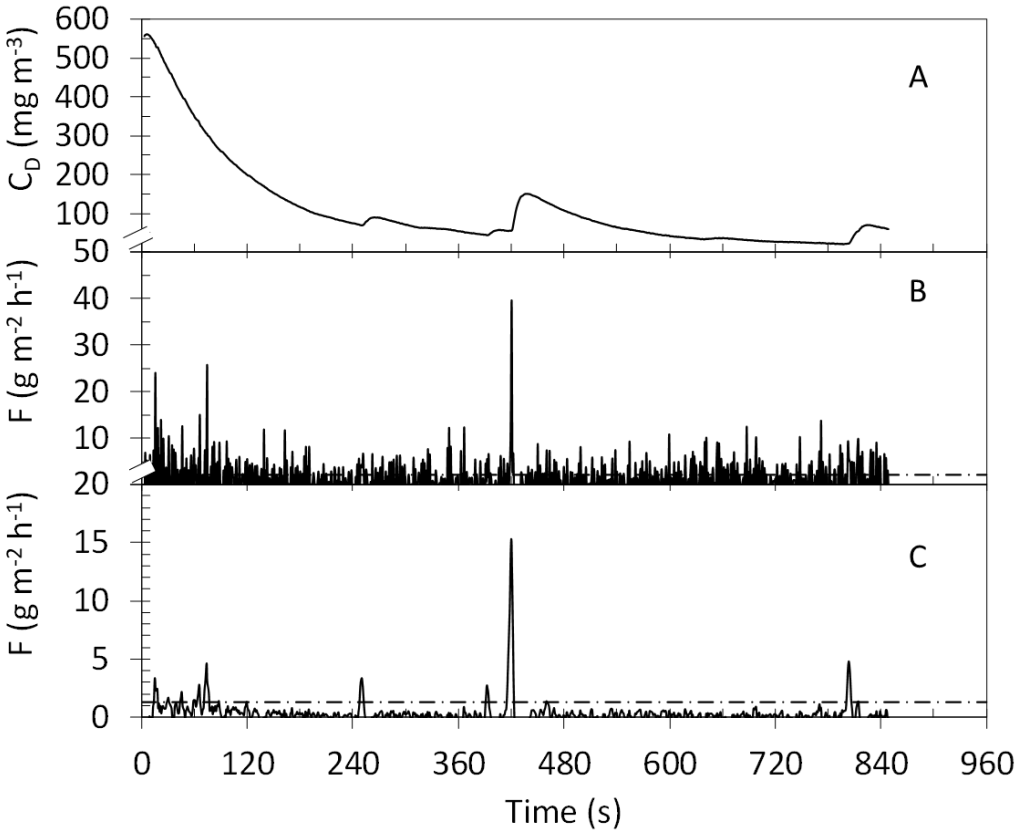

Figure S6. Example of continuous CO_2 flux measurement by ODC in Lake Guadalupe; A. C_D as measured; B. unfiltered flux (Eq. 1); C. double smoothened flux (Eq. 2, 3). Horizontal line in panel B shows the cut-off index.

S7.3 Long term measurement of CH_4 emissions

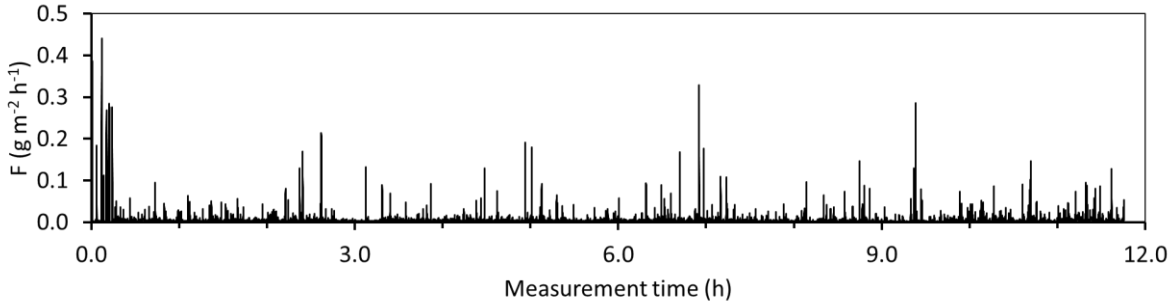

Figure S7. Total CH_4 flux observed over a 12-h continuous measurement. Time 0 corresponds to midnight in such manner that the time corresponds to the hour of the day.

Table S3: Mean (± 1 standard deviation) of total, diffusive and ebullitive flux (mg m^{-2} h^{-1}) observed over three distinctive periods of the day. Means and standard deviations were determined by equally weighted running means of 15 minutes data subsets.

Time period	Time period	Total Flux	Diffusive flux	Ebullitive flux
Night	0:00-3:00	6.0 ± 17.4	3.4 ± 2.1	2.5 ± 17.6
Morning	9:00-12:00	5.2 ± 10.9	2.9 ± 2.5	2.3 ± 11.0
Afternoon	15:00-18:00	5.0 ± 8.4	3.5 ± 2.1	1.5 ± 8.7
	Total	5.3 ± 11.7	3.4 ± 2.2	1.9 ± 11.9

Table S4: Comparison between ODC and other point flux measurement methods.

	Boundary Layer[29]	Bubbles traps[30]	Hydroacoustic bubble detection[21]	Bubble survey[31]	Sensor on robotic boat[32]	Closed static chamber[13]	Closed dynamic chamber[13]	Open dynamic chamber
Ebullitive flux	No	Yes	Yes	Yes	Yes	No	Yes	Yes
Diffusive flux	Yes	No	No	No	No	Yes	Yes	Yes
Distinction ebullitive/diffusive flux	No	No	No	No	No	No	Yes/No [a]	Yes
Continuous measurement	Yes	Yes/No	Yes	No	Yes	No	Yes/No	Yes
Headspace concentration build-up	No	Yes	No	No	No	Yes	Yes	Moderate [b]
Cost (excluding detector) [c]	Low	Low	-	Low	High	Low	Low	Low
Detector sensitivity [d]	High	Low	High	None	High	Moderate/high	Moderate/high	High
Ease of field deployment	High	Moderate	Moderate	High	High	High	High	High
Mobility	High [e]	Low	High [e]	High	High	Moderate	Moderate	Moderate
Direct measurement [f]	No	Yes	No	No	No	Yes	Yes	Yes
High throughput method	Yes	Yes/No	Yes	No	Yes	No	No	Yes
Ancillary measurements	Yes [g]	No	No	No	No	No	No	No
Requirement of carrier gas	No	No	No	No	No	No	No	Yes

[a] *Distinction between diffusive and ebullitive flux is possible, only with relatively high frequency measurements.*
[b] *The continuous carrier gas flow reduces but does not avoid concentration build-up inside the chamber headspace.*
[c] *The experimental set-up, excluding the gas detector is usually of low cost.*
[d] *The detector sensitivity required depends on the level of emissions. Bubbles traps usually require a sensitivity in the % v/v range, while the other methods require a sensitivity in the ppb-ppm v/v range.*
[e] *These methods allow for measurements in motion.*[33]
[f] *Direct measurement refers to the capture of the gas emitted, in an enclosure.*
[g] *The boundary layer method requires the precise measurement of wind speed.*

REFERENCES

(1) Edwards, N. T.; Sollins, P. Continuous measurement of carbon dioxide evolution from partitioned forest floor components. *Ecol. Soc. Am*. **1973**, 54 (2), 406–412.

(2) Denmead, O. T. Chamber systems for measuring nitrous oxide emission from soils in the field. *Soil Sci. Soc. Am. J.* **1979**, 43 (1), 89.

(3) Svensson, L. A new dynamic chamber technique for measuring ammonia emissions from land- spread manure and fertilizers. *Acta Agric. Scand*. **1994**, 35–46.

(4) Fang, C.; Moncrieff, J. B. An improved dynamic chamber technique for measuring CO_2 efflux from the surface of soil. *Funct. Ecol*. **1996**, 10 (2), 297–305.

(5) Gao, F.; Yates, S. R.; Yates, M. V.; Gan, J.; Ernst, F. F. Design, fabrication, and application of a dynamic chamber for measuring gas emissions from soil. *Environ. Sci. Technol*. **1997**, 31 (1), 148–153.

(6) Gao, F.; Yates, S. R. Simulation of enclosure-based methods for measuring gas emissions from soil to the atmosphere. J. *Geophys. Res*. **1998**, 103, 126–129.

(7) Gao, F.; Yates, S. R. Laboratory study of closed and dynamic flux chambers: experimental results and implications for field application. *J. Geophys. Res*. **1998**, 103, 115–125.

(8) Carpi, A.; Lindberg, S. E. Application of a Teflon® dynamic flux chamber for quantifying soil mercury flux: tests and results over background soil. *Atmos. Environ.* **1998**, 32 (5), 873–882.

(9) Zhang, H.; Lindberg, S. E.; Barnett, M. O.; Vette, A. F.; Gustin, M. S. Dynamic flux chamber measurement of gaseous mercury emission fluxes over soils. Part 1: Simulation of gaseous mercury emissions from soils using a two-resistance. *Atmospheric Environment*. **2002**, pp 835–846.

(10) Lindberg, S. E.; Zhang, H.; Vette, A. F.; Gustin, M. S.; Barnett, M. O.; Kuiken, T. Dynamic flux chamber measurement of gaseous mercury emission fluxes over soils: Part 2 - Effect of flushing flow rate and verification of a two-resistance exchange interface simulation model. *Atmospheric Environment*. **2002**, pp 847–859.

(11) Tabachow, R. M.; Roelle, P. A.; Peirce, J. J.; Aneja, V. P. Soil nitric oxide emissions: Lab and field measurements and comparison. *Environ. Eng. Sci*. **2002**, 19 (4), 205–214.

(12) Reichman, R.; Rolston, D. E. Atmospheric pollutants and trace gases design and performance of a dynamic gas flux chamber. *J. Environ. Qual*. **2002**, 31, 1774–1781.

(13) Pumpanen, J.; Kolari, P.; Ilvesniemi, H.; Minkkinen, K.; Vesala, T.; Niinistö, S.; Lohila, A.; Larmola, T.; Morero, M.; Pihlatie, M.; Janssens, I.; Curiel Yuste, Jorge.; Grünzweig, J. M.; Reth, S.; Subke, J.; Savage, K.; Kutsch, W.; Østreng, G.; Zeigler, W.; Anthoni, P.; Lindroth, A.; Hari, P. Comparison of different chamber techniques for measuring soil CO_2 efflux. *Agric. For. Meteorol*. **2004**, 123 (3–4), 159–176.

(14) Denmead, O. T. Approaches to measuring fluxes of methane and nitrous oxide between landscapes and the atmosphere. *Plant Soil*. **2008**, 309 (1–2), 5–24.

(15) Pape, L.; Ammann, C.; Nyfeler-Brunner, A.; Spirig, C.; Hens, K.; Meixner, F. X. An automated dynamic chamber system for surface exchange measurement of non-reactive and reactive trace gases of grassland ecosystems. *Biogeosciences*. **2009**, 6 (3), 405–429.

(16) Breuninger, C.; Oswald, R.; Kesselmeier, J.; Meixner, F. X. The dynamic chamber method: Trace gas exchange fluxes (NO, NO_2, O_3) between plants and the atmosphere in the laboratory and in the field. *Atmos. Meas. Tech.* **2012**, 5 (5), 955–989.

(17) Yu, Z.; Slater, L. D.; Schäfer, K. V. R.; Reeve, A. S.; Varner, R. K. Dynamics of methane ebullition from a peat monolith revealed from a dynamic flux chamber system. *J. Geophys. Res. Biogeoscience*s. **2014**, 119 (9), 1789–1806.

(18) Marasco, D. E.; Hunter, B. N.; Culligan, P. J.; Ga, S. R.; Mcgillis, W. R. Quantifying evapotranspiration from urban green roofs: A comparison of chamber measurements with commonly used predictive methods. *Environ. Sci. Technol.* **2014**, 48, 10273-10281.

(19) Verginelli, I.; Pecoraro, R.; Baciocchi, R. Using dynamic flux chambers to estimate the natural attenuation rates in the subsurface at petroleum contaminated sites. *Sci. Total Environ*. **2018**, 619–620, 470–479.

(20) Rasilo, T.; Prairie, Y. T.; Del Giorgio, P. A. Large-scale patterns in summer diffusive CH_4 fluxes across boreal lakes, and contribution to diffusive C emissions. *Glob. Chang. Biol*. **2015**, 21, 1124–1139.

(21) Ostrovsky, I.; Mcginnis, D. F.; Lapidus, L.; Eckert, W. Quantifying gas ebullition with echosounder: the role of methane transport by bubbles in a medium-sized lake. *Limnol. Oceanogr. Methods*. **2008**, 6 (2), 105–118.

(22) Delwiche, K. B.; Hemond, H. F. Methane bubble size distributions, flux, and dissolution in a freshwater lake. *Environ. Sci. Technol*. **2017**, 51 (23), 13733–13739.

(23) Delwiche, K.; Senft-Grupp, S.; Hemond, H. A novel optical sensor designed to measure methane bubble sizes in situ. *Limnol. Oceanogr. Methods.* **2015**, 13 (12), 712–721.

(24) Delsontro, T.; McGinnis, D. F.; Wehrli, B.; Ostrovsky, I. Size does matter: Importance of large bubbles and small-scale hot spots for methane transport. *Environ. Sci. Technol*. **2015**, 49 (3), 1268–1276.

(25) Martinez, D.; Anderson, M. A. Methane production and ebullition in a shallow, artificially aerated, eutrophic temperate lake (Lake Elsinore, CA). *Sci. Total Environ*. **2013**, 454–455, 457–465.

(26) Sepulveda-Jauregui, A.; Anthony Walter, K. M.; Martinez-Cruz, K.; Greene, S.; Thalasso, F. Methane and carbon dioxide emissions from 40 lakes along a north – south latitudinal transect in Alaska. *Biogeosciences*. **2015**, 12, 3197–3223.

(27) Casper, P.; Maberly, S. C.; Hall, G. H.; Finlay, B. J. Fluxes of methane and carbon dioxide from a small productive lake to the atmosphere. *Biogeochemistry*. **2000**, 49 (1), 1–19.

(28) Poissant, L.; Constant, P.; Pilote, M.; Canário, J.; O'Driscoll, N.; Ridal, J.; Lean, D. The ebullition of hydrogen, carbon monoxide, methane, carbon dioxide and total gaseous mercury from the Cornwall Area of Concern. *Sci. Total Environ*. **2007**, 381 (1–3), 256–262.

(29) Bartosiewicz, E.; Laurion, I.; MacIntyre, S. Greehouse gas emisión and storage in a small shallow lake. *Hydrobiologia*. **2015**, 757(1), 101-115.

(30) Flury, S.; McGinnis, D.; Gessner, M. Methane emissions from a freshwater marsh in response to experimentally simulated global warming and nitrogen enrichment. *J. Geophys. Res.* **2010**, 115(G1), 1-9.

(31) Walter Anthony, K. M.; Vas, D. A.; Brosius, L.; Chapin III, F. S.; Zimov, S. A.; Zhuang, Q. Estimating methane emissions from northern lakes using ice- bubble surveys. *Limnol. Oceanogr.: Methods* **2010**, *8*, 592–609.

(32) Grinham, A.; Dunbabin, M.; Gale, D.; Udy, J. Quantification of ebullitive and diffusive methane release to atmosphere from a water storage. *Atmos. Environ.* **2011**, *45* (39), 7166–7173.

(33) Crawford, J.; Loken, L.; Casson, N.; Smith, C.; Stone, A.; Winslow, L. High-Speed limnology: Using advanced sensors to investigate spatial variability in biogeochemistry and hydrology. *Environ. Sci. Technol.* **2015**, 49, 442-450.